Applied Physics A (2023) 129:349
https://doi.org/10.1007/s00339-023-06636-8

Applied Physics A
Materials Science & Processing

Effect of alumina content on the mechanical properties of alumina-toughened calcia-stabilized tetragonal zirconia ceramic made of baddeleyite

Vyacheslav V. Rodaev[1] · **Svetlana S. Razlivalova**[1]

Received: 14 January 2023 / Accepted: 10 April 2023 / Published online: 15 April 2023

Abstract
Alumina-toughened calcia-stabilized tetragonal zirconia ceramics are produced using baddeleyite as raw material. A 3 wt.% $CaO\text{-}ZrO_2/Al_2O_3$ ceramic containing 15 wt.% Al_2O_3 is characterized by sufficiently high mechanical properties: a hardness of 12.6 GPa, Young's modulus of 248 GPa and fracture toughness of 10.3 $MPa{\cdot}m^{0.5}$. The hardness and Young's modulus of this ceramic exceed those of alumina-free 3 wt.% $CaO\text{-}ZrO_2$ ceramic by about 8.6% and 9.3%, respectively. However, fracture toughness of the prepared composite ceramic is lower than that of 3 wt.% $CaO\text{-}ZrO_2$ ceramic by about 13.7%. It is revealed that in the fabricated 3 wt.% $CaO\text{-}ZrO_2/Al_2O_3$ ceramic in the range of used Al_2O_3 concentrations transformation toughening prevails over residual stress toughening and crack deflection toughening.

Keywords Zirconia ceramic · Baddeleyite · Alumina · High-energy milling · Phase composition · Mechanical properties

1 Introduction

Alumina-toughened zirconia (ATZ) ceramics are composite ceramics for structural applications exhibiting a combination of high fracture toughness due to zirconia component and high strength, hardness, corrosion and wear resistance due to alumina component [1–3]. The hardness and fracture toughness of such composite ceramics are higher than those of alumina, silicon nitride, and silicon carbide ones [4, 5]. ATZ ceramics typically consist of alumina particles dispersed in a tetragonal zirconia polycrystalline (TZP) matrix. Alumina is aluminium oxide in the $\alpha\text{-}Al_2O_3$ phase.

Pure zirconia exhibits three allotropic forms: monoclinic ($m\text{-}ZrO_2$), tetragonal ($t\text{-}ZrO_2$) and cubic ($c\text{-}ZrO_2$) [6]. The $m\text{-}ZrO_2$ phase exists below 1170 °C. The $t\text{-}ZrO_2$ phase is stable in the temperature range of 1170–2370 °C and then transforms into the $c\text{-}ZrO_2$ phase. Upon cooling, the transformation of $t\text{-}ZrO_2$ into $m\text{-}ZrO_2$ is accompanied by a significant increase in volume (approximately 4.5%), which leads to cracking of pure ZrO_2 ceramics [6]. To prevent $t\text{-}ZrO_2 \rightarrow m\text{-}ZrO_2$ phase transition, zirconia is doped with some oxides (Y_2O_3, CeO_2, CaO, and etc.) to stabilize $t\text{-}ZrO_2$ at temperatures below 1170 °C [6].

Typically, stabilized zirconia ceramics are manufactured from powders chemically prepared from precursors of zirconia and stabilizing agent [7, 8]. Chemical approaches are also used to fabricate zirconia nanopowders and for other applications, in particular, to produce thin dielectric films [9], optical sensors [10], catalysts [11], adsorbents for the removal of various water contaminants [12], and etc.

Baddeleyite is a zirconia mineral containing $m\text{-}ZrO_2$, but chemical ways of stabilizing are not efficient for baddeleyite. In [13], wet high-energy milling was successfully applied to baddeleyite to prepare CaO-stabilized ZrO_2 nanopowders, which were used to produce both macroporous and dense spherical zirconia ceramics by the spherification method [14, 15]. In [16], the CaO-stabilized ZrO_2 nanopowder obtained in this way was also used to manufacture calcia-stabilized TZP (Ca-TZP) ceramic by uniaxial pressing and sintering at 1300 °C with good mechanical properties: a hardness of about 11.5 GPa, fracture toughness of about 12 $MPa{\cdot}m^{0.5}$ and Young's modulus of about 230 GPa.

Well known and commercially used yttria-stabilized TZP (Y-TZP) ceramics have low resistance to hydrothermal degradation and thus are not intended for prolonged use in

✉ Vyacheslav V. Rodaev
rodaev1980@mail.ru

[1] Institute for Nanotechnology and Nanomaterials, Derzhavin Tambov State University, 33 Internatsionalnaya Str., 392000 Tambov, Russia

humid environment. Hydrothermal degradation causes a spontaneous t-$ZrO_2 \rightarrow$ m-ZrO_2 phase transition, which leads to cracking and destruction of zirconia ceramics [17]. As an alternative to Y-TZP ceramics ceria-stabilized TZP (Ce-TZP) ceramics are considered [3]. Due to the tetravalent character of cerium, zirconia can be stabilized without generating oxygen vacancies, which facilitate the diffusion of water species into the crystalline lattice of zirconia grains. However, Ce-TZP ceramics have lower fracture strength than Y-TZP ones (500 MPa vs. 1000 MPa), which is partly related to larger grain size (~ 2 µm compared to ~ 0.3 µm for Y-TZP ceramics) [18].

In [19], it was reported that Ca-TZP ceramics are more resistant to hydrothermal degradation compared to Y-TZP ceramics due to smaller grain size. Thus, Ca-TZP ceramics with competitive mechanical properties may be considered as a suitable replacement in biomedical applications for Y-TZP ceramics, which typically have a hardness of 12–13 GPa, Young's modulus of about 210 GPa and fracture toughness of 7–10 MPa·$m^{0.5}$ [20]. Additionally, CaO is much cheaper than Y_2O_3 and CeO_2, and Ca-TZP ceramics require lower sintering temperatures compared to Y-TZP and Ce-TZP ones [21, 22].

In [23], it was observed that ATZ ceramics with Y-TZP matrix are not only less susceptible to hydrothermal aging, but even exhibit an increasing strength during ageing, presumably due to compressive stresses caused by phase transformation, compared to monolithic Y-TZP ceramics.

This study is aimed to obtaining alumina-toughened Ca-TZP ceramic made of baddeleyite with sufficient mechanical characteristics.

2 Materials and methods

We used γ-Al_2O_3 nanopowder (20 nm, Sigma-Aldrich, USA), CaO powder (Sigma-Aldrich, USA) and baddeleyite concentrate powder with zirconia content of 99.3% (5 µm, Kovdorsky mining and processing plant, Russia). The wet high-energy co-milling was carried out on a Pulverisette 7 Premium Line planetary mill (Fritsch, Germany) in the same way as described in [13]. The obtained composite powders contained 0–15 wt.% Al_2O_3. In all the prepared powders the content of CaO was the same and equaled 3 wt% with respect to the CaO-ZrO_2 mixture. The average size of zirconia nanoparticles in the obtained powders was estimated from the X-ray diffraction (XRD) pattern according to the Scherrer equation and was about 20 nm.

The prepared powders were uniaxially pressed under 560 MPa into pellets of a 10 mm diameter and a 2 mm thickness. The obtained pellets were sintered at 1300 °C for 4 h in air atmosphere in a muffle furnace in the same way as in [16].

The crystalline phases were determined with the help of an X-ray diffractometer D2 Phaser (Bruker AXS, Germany). The data were registered over a 2θ range of 20–80°. The obtained XRD patterns were interpreted using the PDF-2 Diffraction Database File compiled by the International Centre for Diffraction. Phase content was calculated from the XRD patterns by the Rietveld method in the TOPAS software (Bruker AXS, Germany).

The elemental composition of ceramics and the spatial distribution of elements in ceramics were analyzed by an energy-dispersive X-ray spectroscopy (EDS) on an INCA Energy 350X-Max 80 spectrometer (Oxford Instruments, UK).

The hardness (H_V) of ceramics was measured automatically by the Vickers indentation method on a Duramin A300 hardness tester (Struers, Denmark) at a loading force of 19.62 N and loading time of 15 s, respectively, using Eq. (1).

$$H_V = 1.8544 \frac{F}{\left(\frac{d_1+d_2}{2}\right)^2} \tag{1}$$

where F is the loading force, d_1 and d_2 are the two diagonal lines of the indentation.

The fracture toughness of ceramics was also measured by the Vickers indentation method using a Duramin A300 hardness tester (Struers, Denmark) at a loading force of 294.3 N. Equation (2) was used to calculate the indentation fracture toughness of ceramics [24].

$$K_C = 0.016 \left(\frac{E}{H_V}\right)^{0.5} \frac{F}{C^{1.5}} \tag{2}$$

where F is the loading force, H_V is the Vickers hardness, E is Young's modulus and C is the crack length, which is the distance between the indentation center and the crack tip. The crack length was determined using an Axio Observer. A1m optical microscope (Carl Zeiss, Germany) equipped with an image capture system.

The Young's modulus of ceramics was measured on a nanoindentometer G200 (MTS Nano Instruments, USA) using a Berkovich diamond indenter and calculated from the load-penetration depth curves obtained under peak load of 5 N using the Oliver–Pharr method [25].

All the samples were polished with diamond-containing slurries prior to the tests.

The Vickers hardness (H_V) and Young's modulus (E) of ceramics are the average of ten effective measurements. The indentation fracture toughness (K_C) of ceramics is the average of five effective measurements.

All measurements were carried out at room temperature.

3 Results and discussion

Figure 1a, b show the hardness and Young's modulus of 3wt.% CaO-ZrO_2/Al_2O_3 ceramic as a function of Al_2O_3 content. It is revealed that the hardness and Young's modulus of a composite ceramic increase linearly with the rise in Al_2O_3 content. If an alumina-free calcia-stabilized zirconia ceramic is characterized by the hardness of 11.6 GPa and Young's modulus of 227 GPa, then for the composite ceramic containing 15 wt.% Al_2O_3 they are 12.6 GPa and 248 GPa, respectively.

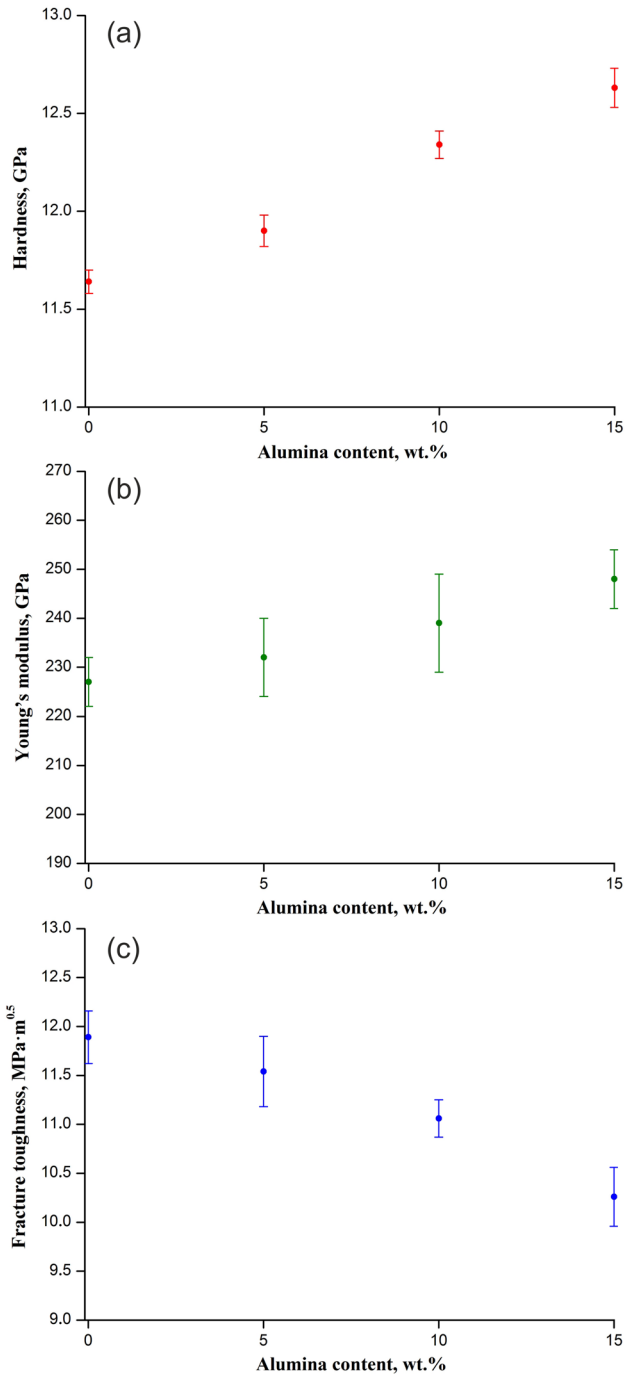

Fig. 1 The mechanical characteristics of 3wt.% CaO-ZrO_2/Al_2O_3 ceramic with different Al_2O_3 content: hardness (**a**), Young's modulus (**b**) and fracture toughness (**c**)

The observed behavior of the hardness and Young's modulus of 3wt.% CaO-ZrO_2/Al_2O_3 ceramic obeys the linear rule of mixtures, which is typical for alumina-toughened zirconia and zirconia-toughened alumina ceramics [26, 27]. The hardness and Young's modulus of monolithic alumina ceramic reach 22 GPa and 380 GPa, respectively, which is much higher than those of stabilized zirconia ceramics [20]. Therefore, it explains the increase in the hardness and Young's modulus of 3wt.% CaO-ZrO_2/Al_2O_3 composite ceramic with increasing Al_2O_3 content.

Figure 1c shows fracture toughness of 3wt.% CaO-ZrO_2/Al_2O_3 ceramic as a function of Al_2O_3 content. The fracture toughness decreases from 11.9 to 10.3 MPa·$m^{0.5}$ with an increase in Al_2O_3 content from 0 to 15 wt.%. A possible reason for the decrease in fracture toughness is discussed below.

The fabricated alumina-toughened calcia-stabilized tetragonal zirconia ceramic with hardness of 12.6 GPa, Young's modulus of 248 GPa and fracture toughness of 10.3 MPa·$m^{0.5}$ is competitive with ATZ ceramics previously fabricated at higher sintering temperatures using commercial powders and traditional stabilizer such as Y_2O_3 and CeO_2. In [26], ATZ ceramic produced from nanopowders of 3 mol% Y_2O_3 stabilized ZrO_2 and Al_2O_3 by cold isostatic pressing followed by sintering at 1550 °C had hardness of 13.2 GPa, Young's modulus of 239 GPa and fracture toughness of 9.3 MPa·$m^{0.5}$. In [28], ATZ ceramic produced from submicron powders of 3 mol% Y_2O_3 stabilized ZrO_2 and Al_2O_3 by uniaxial pressing followed by sintering at 1550 °C was characterized by hardness of 12.5 GPa and fracture toughness of 6.7 MPa·$m^{0.5}$. In [29], powder based on ZrO_2 nanoparticles, doubly doped with CeO_2 and Y_2O_3 and reinforced with Al_2O_3 nanoparticles, was uniaxially pressed and sintered at 1500 °C to produce ATZ ceramic with hardness of 13.9 GPa, Young's modulus of 228 GPa and fracture toughness of 11.3 MPa·$m^{0.5}$. The authors of [30] reported on ATZ ceramic with hardness of 12.4 GPa and fracture toughness of 12.5 MPa·$m^{0.5}$ made of fine powders of m-ZrO_2, Al_2O_3 and CeO_2 uniaxially pressed and sintered at 1600 °C.

The EDS analysis of the fabricated composite ceramic revealed that the material contains only zirconium, aluminium, calcium and oxygen in detectable amounts (Fig. 2a). No segregated regions of zirconium and aluminium were detected by means of EDS mapping (Fig. 2b, c), which allows one to conclude that Al_2O_3 is uniformly distributed in the ZrO_2 matrix.

Figure 3 presents the XRD patterns registered for 3wt.% CaO-ZrO_2/Al_2O_3 ceramics with various Al_2O_3 contents. It

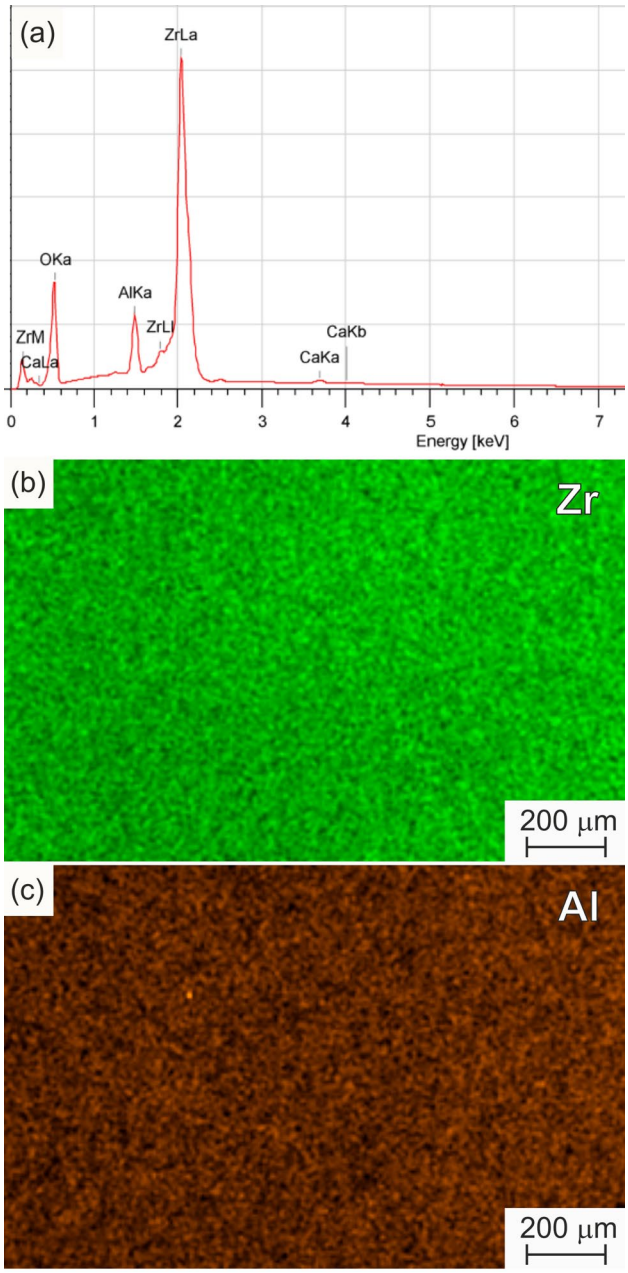

Fig. 2 The results of EDS analysis of 3wt.% CaO-ZrO_2/Al_2O_3 ceramic containing 15 wt.% Al_2O_3 (**a**); EDS mapping of Zr and Al in a 3wt.% CaO-ZrO_2/Al_2O_3 ceramic containing 15 wt.% Al_2O_3 (**b**, **c**)

can be seen that regardless of Al_2O_3 concentration in the range of 0–15 wt.% the composite ceramic contains only characteristic peaks of t-ZrO_2 located at 30.2°, 34.6°, 35.2°, 50.2°, 50.7°, 59.3°, and 60.2°. This indicates that we are dealing with composite ceramic with a TZP matrix. The absence of alumina reflections in the XRD patterns can probably be explained by the significantly higher intensity of the t-ZrO_2 peaks or the much smaller grain size of α-Al_2O_3 compared to t-ZrO_2. The main characteristic peaks

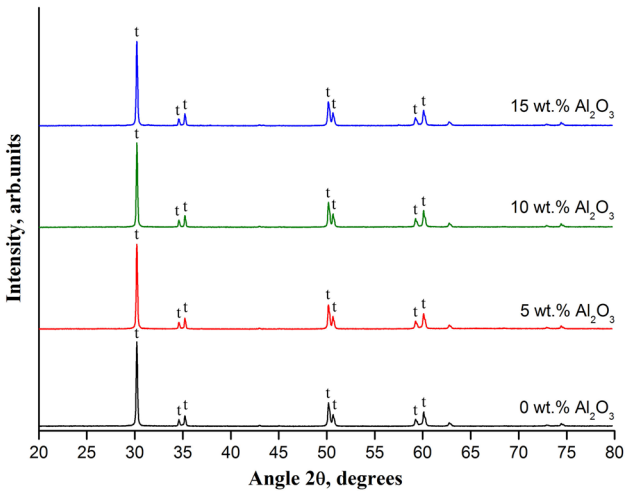

Fig. 3 The XRD patterns of 3wt.% CaO-ZrO_2/Al_2O_3 ceramic with different Al_2O_3 content

of α-Al_2O_3 are located near 25.6°, 35.1°, 43.4°, and 57.5°. It should be noted that at temperatures above 1100 °C aluminium oxide can exist only in the α-Al_2O_3 phase [31]. We believe that aluminium oxide doesn't dissolve significantly in Ca-TZP to form a solid solution, since there is no noticeable shift of diffraction peaks, as was observed in [32] due to formation a solid solution of Nb_2O_5 in Y-TZP. In [33], it was reported that aluminium oxide was dissolved only up to 0.18 wt.% in Y-TZP at 1400 °C. The XRD spectrum of 10 wt.% Al_2O_3-ZrO_2 ceramic (Fig. 4) confirms that aluminium oxide is not a stabilizer, since the obtained calcia-free zirconia ceramic contains mainly m-ZrO_2 with a fraction of t-ZrO_2 less than 5%. The Scherrer equation was applied to the most intense peak of t-ZrO_2 at 30.2° to estimate the average

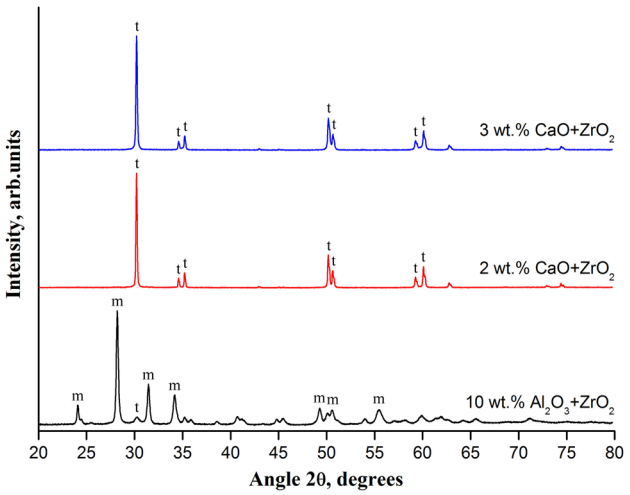

Fig. 4 The XRD patterns of zirconia ceramics stabilized by CaO and Al_2O_3

t-ZrO_2 grain size in a 3 wt.% CaO-ZrO_2/Al_2O_3 ceramic with different Al_2O_3 content (Table 1).

According to Table 1 the average t-ZrO_2 grain size decreases from 78 to 69 nm as alumina content increases from 0 to 15% in the fabricated ATZ ceramic. A decrease in the average zirconia grain size accompanied by an increase in the content of alumina in the composite ceramic is probably a manifestation of the pinning effect, when fine particles dispersed in the matrix prevent the movement of grain boundaries through a polycrystalline material by exerting a pinning pressure which counteracts the driving force pushing the boundaries [27]. In our case, alumina grains distributed over the entire zirconia matrix and predominantly located at triple junctions [4] limit the growth of matrix grains. Obviously, the higher the inclusions content is, the more it affects the growth of matrix grains.

It should be noted that the observed increase in the hardness of 3 wt.% CaO-ZrO_2/Al_2O_3 ceramic accompanied by a decrease in the average t-ZrO_2 grain size cannot be explained within the framework of the Hall–Petch theory, according to which the hardness (or strength) of a polycrystalline material increases with the decrease in its grain size:

$$H = H_0 + kD^{-0.5} \quad (3)$$

where H is the measured hardness, H_0 is the intrinsic hardness related to the resistance of lattice to dislocation motion, k is a constant specific for each material also known as the Hall–Petch parameter, and D is the average grain size.

The observed dependence of the hardness of 3 wt.% CaO-ZrO_2/Al_2O_3 ceramic on the inversed square root of the average t-ZrO_2 grain size (Fig. 5) is not linear as required by the Hall–Petch relationship (3).

The Hall–Petch effect was observed on the hardness of submicro- and nanograined Y-TZP ceramics sintered at different temperatures [34], where t-ZrO_2 grain growth was stimulated by increasing the sintering temperature.

It was found that phase composition of 2 wt.% CaO-ZrO_2/Al_2O_3 ceramic depends on Al_2O_3 content in contrast to 3 wt.% CaO-ZrO_2/Al_2O_3 ceramic. If alumina-free 2 wt.% CaO-ZrO_2 ceramic consists only of t-ZrO_2 grains, then the rise in Al_2O_3 content leads to a reduction of t-ZrO_2 content and an increase in m-ZrO_2 content (Fig. 6). The

Table 1 The average t-ZrO_2 grain size in a 3 wt.% CaO-ZrO_2/Al_2O_3 ceramic with different Al_2O_3 content

Al_2O_3 content, wt.%	Average t-ZrO_2 grain size, nm
0	78
5	76
10	72
15	69

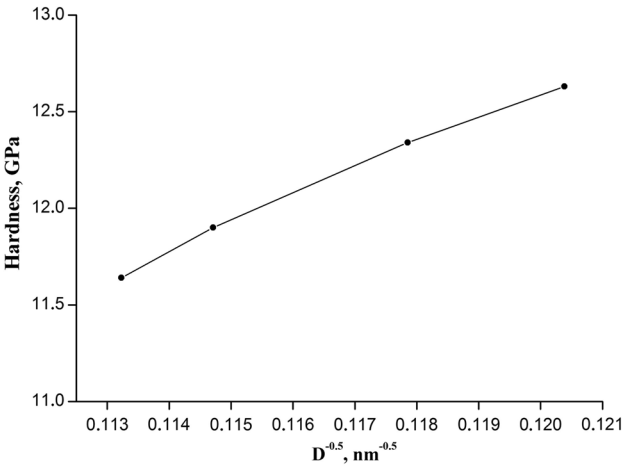

Fig. 5 The dependence of the hardness of 3 wt.% CaO-ZrO_2/Al_2O_3 ceramic with different Al_2O_3 content on the inversed square root of the average t-ZrO_2 grain size. The dots are connected by lines for clarity

characteristic peaks of m-ZrO_2 appear in the XRD patterns, the intensity of which increases with increasing Al_2O_3 content. An increase in Al_2O_3 concentration from 0 to 10 wt.% leads to an increase in m-ZrO_2 content from 0 to 93%. In [16], the authors reported that 1 wt.% CaO-ZrO_2 ceramic sintered at 1300 °C contained more than 90% m-ZrO_2. This allows us to conclude that part of CaO (up to about 1 wt.%) reacts with Al_2O_3 during ceramic sintering to form calcium aluminates [35], which leads to a decrease in the content of the stabilizing agent. This results in the appearance of m-ZrO_2 in a 2 wt.% CaO-ZrO_2/Al_2O_3 ceramic.

The decreasing tendency of fracture toughness of 3 wt.% CaO-ZrO_2/Al_2O_3 ceramic with an increase in Al_2O_3 content shown in Fig. 1c is closely related to the fraction of

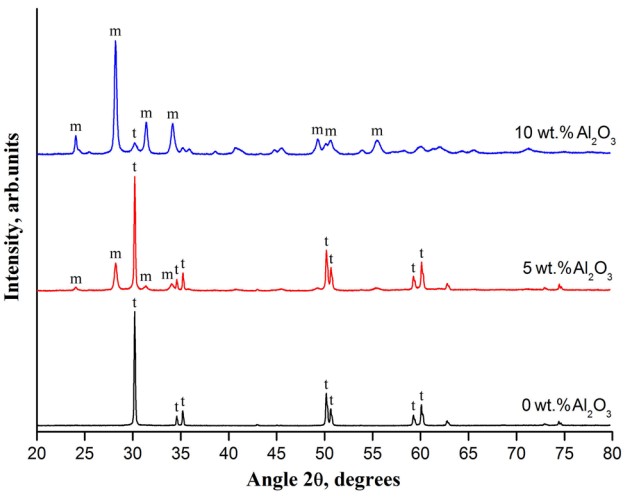

Fig. 6 The XRD patterns of 2 wt.% CaO-ZrO_2/Al_2O_3 ceramic with different Al_2O_3 content

the transformable t-ZrO_2 phase. Indeed, the rise in Al_2O_3 concentration leads to a decrease in the content of t-ZrO_2, which negatively affects transformation toughening. Transformation toughening is activated by stresses at the tip of a propagating crack inducing t-$ZrO_2 \rightarrow$ m-ZrO_2 phase transition [36]. This is accompanied by a volume expansion of the zirconia grains, which prevents the crack propagation due to induced compressive stress. Stress-induced transformation is the most important toughening mechanism in stabilized zirconia ceramics [37].

In addition to a decrease in the amount of t-ZrO_2, the grain size of t-ZrO_2 also decreases with the rise in Al_2O_3 content (Table 1). For a given stabilizing agent concentration the ability of t-ZrO_2 grains to perform phase transition reduces as t-ZrO_2 grain size decreases [37]. The over-stabilization effect makes the t-$ZrO_2 \rightarrow$ m-ZrO_2 phase transition impossible, when a crack is introduced. On the other hand, with an increase in the t-ZrO_2 grain size, the probability of the t-$ZrO_2 \rightarrow$ m-ZrO_2 phase transition increases, which leads to an increase in fracture toughness. In [16], it was reported about Ca-TZP ceramic with the average t-ZrO_2 grain size of 93 nm and fracture toughness of 13.1 MPa·$m^{0.5}$. However, it was found that the t-ZrO_2 grain size cannot exceed 100 nm in Ca-TZP ceramics [38]. Further grain growth results in spontaneous t-$ZrO_2 \rightarrow$ m-ZrO_2 phase transition and ceramic destruction due to cracking.

Alumina grains present in a TZP matrix provide another toughening mechanism that generates residual stress due to the difference in thermal expansion coefficients of alumina and zirconia [39]. Thus, during crack propagation in two-phase regions of ATZ ceramics higher fracture energy is required for the crack to continue propagating.

In addition, uniformly distributed hard alumina grains in a TZP matrix also provide crack deflection toughening, since the transgranular fracture energy of alumina grains is higher than the transgranular fracture energy of zirconia grains, as well as the intergranular fracture energy [39].

The role of residual stress toughening and crack deflection toughening in ATZ ceramics increases with increasing Al_2O_3 content. However, the observed decrease in fracture toughness of 3 wt.% CaO-ZrO_2/Al_2O_3 ceramic with the rise in Al_2O_3 content indicates that in the fabricated ATZ ceramic in the range of used Al_2O_3 concentrations transformation toughening prevails.

4 Conclusions

Alumina-toughened Ca-TZP ceramics are produced using baddeleyite as raw material. A 3 wt.% CaO-ZrO_2/Al_2O_3 ceramic containing 15 wt.% Al_2O_3 is characterized by adequate mechanical properties, namely: hardness of 12.6 GPa, Young's modulus of 248 GPa and fracture toughness of 10.3 MPa·$m^{0.5}$. The hardness and Young's modulus of this ceramic exceed those of alumina-free 3 wt.% CaO-ZrO_2 ceramic by about 8.6% and 9.3%, respectively. However, fracture toughness of the prepared composite ceramic is lower than that of 3 wt.% CaO-ZrO_2 ceramic by about 13.7%. It is revealed that in the fabricated 3 wt.% CaO-ZrO_2/Al_2O_3 ceramic in the range of used Al_2O_3 concentrations transformation toughening prevails over residual stress toughening and crack deflection toughening. Since alumina is not subject to hydrothermal aging, we suppose that alumina-toughed Ca-TZP ceramic is more resistant to hydrothermal degradation than monolithic Ca-TZP ceramic, which is important for biomedical and some structural applications. The investigation of the effect of hydrothermal ageing on the mechanical characteristics of alumina-toughed Ca-TZP ceramic will be the aim of our further research.

Acknowledgements The results were obtained using the equipment of the Center for Collective Use of Scientific Equipment of TSU named after G.R. Derzhavin.

Author contributions Conceptualization, methodology, writing—original draft: Vyacheslav VR; formal analysis and investigation: SSR. All authors read and approved the final manuscript.

Funding The reported study was funded by the Russian Science Foundation grant No.22-29-00119, https://rscf.ru/project/22-29-00119/.

Data availability All data included in this study are available upon request from the corresponding author.

Declarations

Conflict of interest The authors declare no conflict of interest.

Financial interest The authors declare they have no financial interests.

References

1. A. Maji, G. Choubey, Mater. Today: Proc. (2018). https://doi.org/10.1016/j.matpr.2017.11.417
2. E.T.P. Bergamo, K.B. Cardoso, L.F.O. Lino, T.M.B. Campos, K.N. Monteiro, P.F. Cesar, L.A. Genova, G.P. Thim, P.G. Coelho, E.A. Bonfante, J. Biomed. Mater. Res. Part B Appl. Biomater. (2021). https://doi.org/10.1002/jbm.b.34776
3. M.F.R.P. Alves, M.H.F.V. Fernandes, J.K.M.B. Daguano, A.C.D. Rodas, J.E.V. Amarante, C. dos Santos, J. Mech. Behav. Biomed. Mater. (2022). https://doi.org/10.1016/j.jmbbm.2022.105363
4. E.D.S. Lima, C.C. Gall, M.F.R. Alves, J.B. de Campos, T.M.B. Campos, C.D. Santos, J. Mater. Res. Technol. (2022). https://doi.org/10.1016/j.jmrt.2021.11.141
5. A. Moradkhani, H. Baharvandi, Eng. Fract. Mech. (2018). https://doi.org/10.1016/j.engfracmech.2017.12.033
6. O.S.A. El-Ghany, A.H. Sherief, Future Dent. J. (2016). https://doi.org/10.1016/j.fdj.2016.10.002
7. V.B. Kulmeteva, S.E. Porozova, B.L. Krasnyi, V.P. Tarasovskii, A.B. Krasnyi, Refract. Ind. Ceram. (2009). https://doi.org/10.1007/s11148-010-9233-5

8. J. Xiao, Q. Han, F. Yu, Y. Zhang, H. Wu, X. Li, X. Zeng, P. Dong, Y. Zhang, J. Liu, Alloys Compd. (2018). https://doi.org/10.1016/j.jallcom.2017.10.130
9. R.C. Hoffmann, M. Kaloumenos, E. Erdem, S. Weber, J.J. Schneider, Eur. J. Inorg. Chem. (2014). https://doi.org/10.1002/ejic.201402634
10. M. Răileanu, L. Todan, M. Voicescu, N. Drăgan, D. Crişan, M. Maganu, D.M. Vuluga, A. Ianculescu, D.C. Culiţă, Ceram. Int. (2015). https://doi.org/10.1016/j.ceramint.2014.11.128
11. M.F. Hanafi, N. Sapawe, Mater. Today: Proc. (2019). https://doi.org/10.1016/j.matpr.2019.11.180
12. S. Sonal, B.K. Mishra, Chem. Eng. J. (2021). https://doi.org/10.1016/j.cej.2021.130509
13. A.O. Zhigachev, A.V. Umrikhin, Y.I. Golovin, B.Y. Farber, Int. J. Appl. Ceram. Technol. (2015). https://doi.org/10.1111/ijac.12377
14. V.V. Rodaev, V.M. Vasyukov, A.O. Zhigachev, V.V. Korenkov, Yu.I. Golovin, Appl. Phys. A (2019). https://doi.org/10.1007/s00339-019-2541-9
15. V.V. Rodaev, A.O. Zhigachev, V.V. Korenkov, Y.I. Golovin, Mater. Sci. Eng. A (2018). https://doi.org/10.1016/j.msea.2018.06.029
16. V.V. Rodaev, A.O. Zhigachev, A.I. Tyurin, S.S. Razlivalova, V.V. Korenkov, Yu.I. Golovin, Materials (2021). https://doi.org/10.3390/ma14164676
17. K. Matsui, K. Nakamura, M. Saito, A. Kuwabara, H. Yoshida, Y. Ikuhara, Acta Mater. (2022). https://doi.org/10.1016/j.actamat.2022.117659
18. D. Tovar-Vargas, E. Roitero, M. Anglada, E. Jimenez-Pique, H. Reveron, J. Eur. Ceram. Soc. (2021). https://doi.org/10.1016/j.jeurceramsoc.2021.05.006
19. A.O. Zhigachev, A.V. Umrikhin, V.V. Korenkov, Yu.I. Golovin, J. Am. Ceram. Soc. (2017). https://doi.org/10.1111/jace.14844
20. C. Gautam, J. Joyner, A. Gautam, J. Rao, R. Vajtai, Dalton Trans. (2016). https://doi.org/10.1039/C6DT03484E
21. M.F.R.P. Alves, L.Q.B. de Campos, B.G. Simba, C.R.M. da Silva, K. Strecker, C. dos Santos, Ceramics (2022). https://doi.org/10.3390/ceramics5040058
22. W. Zhang, J. Bao, G. Jia, W. Guo, X. Song, S. An, J. Alloys Compd. (2017). https://doi.org/10.1016/j.jallcom.2017.04.059
23. P. Kohorst, L. Borchers, J. Strempel, M. Stiesch, T. Hassel, F.-W. Bach, C. Hübsch, Acta Biomater. (2012). https://doi.org/10.1016/j.actbio.2011.11.016
24. G.R. Anstis, P. Chantikul, B.R. Lawn, D.B. Marshall, J. Am. Ceram. Soc. (1981). https://doi.org/10.1111/j.1151-2916.1981.tb10320.x
25. A.C. Fischer-Cripps, *Nanoindentation*, 3rd edn. (Springer, New York, 2011), p.282
26. D. Tang, K.-J. Lee, J. Xu, H.-B. Lim, K. Park, W.-S. Cho, Met. Mater. Int. (2012). https://doi.org/10.1007/s12540-012-3026-y
27. V. Naglieri, P. Palmero, L. Montanaro, J. Chevalier, Materials (2013). https://doi.org/10.3390/ma6052090
28. F. Zhang, L.-F. Lin, E.-Z. Wang, Ceram. Int. (2015). https://doi.org/10.1016/j.ceramint.2015.06.081
29. C. dos Santos, I.F. Coutinho, J.E.V. Amarante, M.F.R.P. Alves, M.M. Coutinho, C.R.M. da Silva, J. Mech. Behav. Biomed. Mater. (2021). https://doi.org/10.1016/j.jmbbm.2021.104372
30. W.-M. Guo, L.-Y. Zeng, L.-X. Wu, H.-J. Wang, S.-K. Sun, H.-T. Lin, S.-H. Wu, C.-Y. Wang, J. Am. Ceram. Soc. (2017). https://doi.org/10.1111/jace.15379
31. J. Lee, H. Jeon, D.G. Oh, J. Szanyi, J.H. Kwak, Appl. Catal. A Gen. (2015). https://doi.org/10.1016/j.apcata.2015.03.040
32. S.-Y. Yang, J.-H. Lee, J.-J. Kim, J.-S. Lee, Solid State Ion. (2004). https://doi.org/10.1016/j.ssi.2004.03.026
33. E. Sato, H. Morioka, K. Kuribayashi, D. Sundararaman, J. Mater. Sci. (1999). https://doi.org/10.1023/A:1004693306615
34. M. Trunec, Ceram. Silikáty **52**, 165 (2008)
35. M. Zhang, Y. Peng, Y. Sun, P. Li, J. Yu, Fuel (2013). https://doi.org/10.1016/j.fuel.2013.03.078
36. J. Chevalier, L. Gremillard, A.V. Virkar, D.R. Clarke, J. Am. Ceram. Soc. (2009). https://doi.org/10.1111/j.1551-2916.2009.03278.x
37. J.R. Kelly, I. Denry, Dent. Mater. (2008). https://doi.org/10.1016/j.dental.2007.05.005
38. A. Łabuz, R. Lach, M. Rączka, B. Wójtowicz, W. Pyda, J. Eur. Ceram. Soc. (2015). https://doi.org/10.1016/j.jeurceramsoc.2015.06.022
39. Y. Yu, X. Liu, Y. Yuan, W. Yu, H. Yin, Z. Yin, Y. Zheng, X. He, J. Mater. Res. Technol. (2022). https://doi.org/10.1016/j.jmrt.2021.12.057